

Viability of $\Delta m^2 \sim 1 \text{ eV}^2$ sterile neutrino mixing models in light of MiniBooNE electron neutrino and antineutrino data from the Booster and NuMI beamlines

G. Karagiorgi^{1,*}, Z. Djurcic^{2,†}, J. M. Conrad^{1,‡}, M. H. Shaevitz^{2,§} and M. Sorel^{3¶}

¹*Massachusetts Institute of Technology, Cambridge, MA 02139*

²*Department of Physics, Columbia University, New York, NY 10027 and*

³*Instituto de Física Corpuscular, IFIC, CSIC and Universidad de Valencia, Spain*

(Dated: January 6, 2019)

This paper examines sterile neutrino oscillation models in light of recently published results from the MiniBooNE Experiment. The new MiniBooNE data include the updated neutrino results, including the low energy region, and the first antineutrino results, as well as first results from the off-axis NuMI beam observed in the MiniBooNE detector. These new global fits also include data from LSND, KARMEN, NOMAD, Bugey, CHOOZ, CCFR84, and CDHS. Constraints from atmospheric oscillation data have been imposed. We test the validity of the three-active plus one-sterile (3+1) and two-sterile (3+2) oscillation hypotheses, and we estimate the allowed range of fundamental neutrino oscillation parameters in each case. We assume CPT-invariance throughout. However, in the case of (3+2) oscillations, CP violation is allowed. We find that, with the addition of the new MiniBooNE datasets, a (3+2) oscillation hypothesis provides only a marginally better description of all short-baseline data over a (3+1) oscillation hypothesis. For the case of (3+2) CP-violating models, we find that the appearance experiments, MiniBooNE, LSND, KARMEN and NOMAD, provide a satisfactory χ^2 -probability of 27%, but they are incompatible at $\sim 3.8\sigma$. All short-baseline experiments yield a χ^2 -probability of 52% for the best fit hypothesis corresponding to a CPV phase of 1.8π . However, despite the high χ^2 -probability, the incompatibility among appearance and disappearance experiments, and among neutrino and antineutrino experiments, is found to be large, at $\sim 3.0\sigma$ and $\sim 3.3\sigma$, respectively. The datasets responsible for this tension are the MiniBooNE neutrino dataset, CDHS, and the atmospheric constraints. Less tension exists among antineutrino-only experiments, which yield a χ^2 -probability of 87% at the best-fit (3+2) oscillation hypothesis, and 5.8% compatibility.

PACS numbers: 14.60.Pq, 14.60.St, 12.15.Ff

I. INTRODUCTION

Sterile neutrino oscillation models were proposed more than a decade ago as an explanation for the LSND anomaly [1, 2, 3, 4, 5], an excess of events consistent with $\bar{\nu}_\mu \rightarrow \bar{\nu}_e$ oscillations at high Δm^2 . These models relate ν_e appearance with ν_μ and ν_e disappearance, motivating combined fits in all three oscillation channels. Relatively early in the discussion of models, it was demonstrated [5, 6] that a three-active plus one-sterile (3+1) neutrino oscillation model could not reconcile the LSND result with existing null results from other short-baseline (SBL) experiments, including KARMEN [7], NOMAD [8], Bugey [9], CHOOZ [10], CCFR84 [11], and CDHS [12], which had similar high Δm^2 sensitivity. However, it was shown that a three-active plus two-sterile neutrino (3+2) oscillation scenario provided a better description of these datasets [5].

In 2001, the MiniBooNE experiment began running with the goal to test the LSND result using both neutrino and antineutrino beams. This is a short-baseline appearance and disappearance experiment located at Fermi National Accelerator Laboratory (Fermilab). MiniBooNE's first result, reported in 2007, described a search for $\nu_\mu \rightarrow \nu_e$ oscillations [13]. These results were incompatible with a simple two-neutrino oscillation interpretation and, within this model, MiniBooNE excluded the LSND result at the 98% CL. However, this same analysis reported a 3.7σ excess of electron neutrino candidate events at low energies, between 300-475 MeV, which remains unexplained. The MiniBooNE first result was included in a global fit for (3+1) and (3+2) oscillation scenarios in Ref. [14]. This result built on an earlier study, which introduced the possibility of CP violation ($P(\nu_\mu \rightarrow \nu_e) \neq P(\bar{\nu}_\mu \rightarrow \bar{\nu}_e)$) within (3+2) fits [15]. Including the first MiniBooNE results into the global fit led to two observations in Ref. [14]: 1) MiniBooNE, LSND, and the null appearance experiments (KARMEN and NOMAD) are compatible under a (3+2) sterile neutrino oscillation scenario with large CP violation. 2) There is severe tension between appearance and disappearance experiments, at a level of more than 3σ . In this paper we will consider both observations in light of new appearance data. Also, we will show that the incompatibil-

*Electronic address: georgiak@mit.edu

†Electronic address: zdjurcic@nevis.columbia.edu

‡Electronic address: conrad@mit.edu

§Electronic address: shaevitz@nevis.columbia.edu

¶Electronic address: sorel@ific.uv.es

Dataset	Channel	Classification
Appearance experiments:		
LSND	$\bar{\nu}_\mu \rightarrow \bar{\nu}_e$	signal
BNB-MB(ν)	$\nu_\mu \rightarrow \nu_e$	signal
BNB-MB($\bar{\nu}$)	$\bar{\nu}_\mu \rightarrow \bar{\nu}_e$	inconclusive
NUMI-MB	$\nu_\mu \rightarrow \nu_e$	null
KARMEN	$\bar{\nu}_\mu \rightarrow \bar{\nu}_e$	null
NOMAD	$\nu_\mu \rightarrow \nu_e$	null
Disappearance experiments:		
Bugey	$\bar{\nu}_e \rightarrow \bar{\nu}_q$	null
CHOOZ	$\bar{\nu}_e \rightarrow \bar{\nu}_q$	null
CCFR84	$\nu_\mu \rightarrow \nu_\mu$	null
CDHS	$\nu_\mu \rightarrow \nu_\mu$	null

TABLE I: Short-baseline oscillation datasets considered in this paper, and oscillation channel that each dataset constrains. The right column indicates the classification of each dataset: null indicates agreement with a no-oscillation hypothesis; signal indicates disagreement with a no-oscillation hypothesis.

ity between appearance and disappearance experiments arises mainly from two ν_μ disappearance datasets: CDHS and atmospheric constraints.

Motivated by three new results from MiniBooNE, this paper re-examines the (3+1) and (3+2) global fits to the SBL data. These new results are: 1) an updated $\nu_\mu \rightarrow \nu_e$ result [16]; 2) first results for a $\bar{\nu}_\mu \rightarrow \bar{\nu}_e$ search [17]; and 3) first $\nu_\mu \rightarrow \nu_e$ results from the NuMI off-axis beam at MiniBooNE [18]. We consider these new results in combination with seven SBL datasets. These provide constraints on: ν_μ disappearance (from the CCFR84 and CDHS experiments), $\bar{\nu}_e$ disappearance (from the Bugey and CHOOZ experiments), $\nu_\mu \rightarrow \nu_e$ oscillations (from the NOMAD experiment), and $\bar{\nu}_\mu \rightarrow \bar{\nu}_e$ oscillations (from the LSND and KARMEN experiments). Furthermore, we have taken into account atmospheric constraints based on the analysis of Ref. [19]. These constraints have been incorporated in our analysis following the method described in Ref. [15], and are included in fits to all SBL experiments, null SBL experiments, or as explicitly stated. Table I summarizes all SBL datasets used in the fits presented in this paper.

The paper is organized as follows. In Section II, we provide a short description of the MiniBooNE experiment and the new datasets. In Section III, we specify the formalism used in this analysis to describe (3+ n) oscillations, where n is the number of sterile neutrinos. In Section IV, we discuss the analysis method followed, and describe in detail the way in which the three MiniBooNE datasets have been incorporated. In Section V we present the results obtained for the (3+1) (CP-conserving only), and (3+2) CP-conserving and CP-violating hypotheses. For each hypothesis we quote the compatibility between various sets of SBL experiments, and report the best-fit neutrino mass and mixing parameters derived from the combined analysis of all experimental datasets. In the (3+2) CP-violating case we discuss the constraints on

the CP violation phase, inferred from a combined analysis of all SBL oscillation results. Finally, in Section VI we discuss constraints to the (3+2) CP-violating models from each of the SBL experiments considered in this analysis. The goal of this particular study was to investigate whether the source of tension between appearance and disappearance experiments [14] is a result of a single experiment.

II. THE NEW MINIBOOONE DATASETS

The MiniBooNE experiment uses a muon neutrino beam produced by 8 GeV protons from the Fermilab Booster Neutrino Beamline (BNB) impinging on a beryllium target. The target is located within a magnetic focusing horn [20]. The current of the horn can be reversed for running neutrinos or antineutrinos, allowing MiniBooNE to perform both neutrino and antineutrino oscillation searches. The detector [21] is located $L = 541$ m from the primary target, and the neutrino flux has an average energy of ~ 0.75 GeV. This design maintains the LSND $L/E \sim 1$ m/MeV. The detector consists of a spherical tank with active radius 610 cm, instrumented with 1520 8-inch photomultipliers. This is filled with 800 tons of pure mineral oil. An outer veto region rejects cosmic rays and neutrino events producing particles which cross the detector boundaries.

The MiniBooNE neutrino dataset used in this analysis corresponds to the updated results recently reported by the MiniBooNE collaboration [16]. Compared to the first MiniBooNE result which was released in 2007 [13], the new result involves a re-analysis of the MiniBooNE low energy excess events and several updates to the Monte Carlo prediction. These updates include a new model of photonuclear effects, incorporation of new data on π^0 production and a better treatment of pion re-interaction in the detector following decay, an improved estimate and rejection method of the background from interactions outside the detector, and improvements to the determination of systematic errors. The updated low-energy analysis has resulted in a reduction to the significance of the excess from 3.7σ in the original analysis to 3.4σ , along with some slight modification to the shape of the energy spectrum; specifically, the peak of the excess has shifted slightly to higher neutrino energies. In addition, the new analysis extends in energy down to 200 MeV, compared to 300 MeV in the original analysis, which offers additional L/E information. The new result also corresponds to modestly higher statistics, corresponding to the total data collected during the experiment's neutrino running of 6.46×10^{20} protons on target (POT), compared to 5.58×10^{20} , previously.

More recently, the MiniBooNE Collaboration reported their first results from a search for $\bar{\nu}_\mu \rightarrow \bar{\nu}_e$ oscillations, using a muon antineutrino beam [17]. The antineutrino analysis performed by MiniBooNE mirrors the updated neutrino analysis [16], and includes the Monte Carlo pre-

diction updates of the latter. The total antineutrino dataset used in the analysis corresponds to 3.39×10^{20} POT. However, due to production and cross-section effects, the antineutrino event sample, unlike the neutrino event sample, is statistically limited. Unlike the neutrino search, the MiniBooNE antineutrino search provides a direct test of the LSND result. Compared to the results from KARMEN, the MiniBooNE sensitivity to $\bar{\nu}_\mu \rightarrow \bar{\nu}_e$ extends into the low- Δm^2 region allowed by a combined analysis of KARMEN and LSND data. Nevertheless, no conclusive signal has been observed, and a limit has been set; this limit is considerably weaker than the sensitivity, and is comparable to the KARMEN limit. The limit degradation with respect to the sensitivity is due to a 2.8σ fluctuation of data above expected background observed in the 475-675 MeV energy region. Thus, at present, the MiniBooNE antineutrino result is inconclusive with respect to oscillations allowed by LSND. However, MiniBooNE is in the process of collecting more antineutrino data. This is expected to improve the experiment's sensitivity to $\bar{\nu}_\mu \rightarrow \bar{\nu}_e$ oscillations. Updated results are expected after about three years of running.

As suggested in Table I, in the analysis presented in this paper, the MiniBooNE neutrino and antineutrino datasets will be treated as signal experiments, rather than null experiments. This is due to changes associated with the analysis procedure described in Sec. IV.

The third new dataset [18] arises from the fact that the MiniBooNE detector is illuminated by the off-axis (110 mrad) neutrino flux from the NuMI beamline at Fermilab. This analysis has reported a 1.2σ excess of ν_e -like events in the neutrino energy range below 900 MeV. The NuMI dataset corresponds to a mean L/E that is approximately the same as those of the MiniBooNE and LSND datasets, and therefore probes the same Δm^2 range, providing complementary information in oscillation fits with MiniBooNE and LSND.

III. (3+n) STERILE NEUTRINO OSCILLATION FORMALISM

The formalism used in this paper follows that which was presented in Ref. [15]. We provide a brief summary here.

In the sterile neutrino oscillation models, under the assumptions of CPT invariance and negligible matter effects, the probability for a neutrino produced with flavor α and energy E , to be detected as a neutrino of flavor β after traveling a distance L , is given by [22, 23]:

$$P(\nu_\alpha \rightarrow \nu_\beta) = \delta_{\alpha\beta} - 4 \sum_{i>j} \mathcal{R}(U_{\alpha i}^* U_{\beta i} U_{\alpha j} U_{\beta j}^*) \sin^2 x_{ij} + 2 \sum_{i>j} \mathcal{I}(U_{\alpha i}^* U_{\beta i} U_{\alpha j} U_{\beta j}^*) \sin 2x_{ij} \quad (1)$$

where \mathcal{R} and \mathcal{I} indicate the real and imaginary parts of the product of mixing matrix elements, respectively; $\alpha, \beta \equiv e, \mu, \tau$, or s , (s being the sterile flavor); $i, j = 1, \dots, 3+n$ (n being the number of sterile neutrino

species); and $x_{ij} \equiv 1.27 \Delta m_{ij}^2 L/E$. In defining x_{ij} , we take the neutrino mass splitting $\Delta m_{ij}^2 \equiv m_i^2 - m_j^2$ in eV^2 , the neutrino baseline L in km, and the neutrino energy E in GeV. For antineutrinos, the oscillation probability is obtained from Eq. 1 by replacing the mixing matrix U with its complex-conjugate matrix. Therefore, if the mixing matrix is not real, neutrino and antineutrino oscillation probabilities can differ.

For $3+n$ neutrino species, there are, in general, $2+n$ independent mass splittings, $(3+n)(2+n)/2$ independent moduli of parameters in the unitary mixing matrix, and $(2+n)(1+n)/2$ Dirac CP-violating phases that may be observed in oscillations. In SBL neutrino experiments that are sensitive only to $\nu_\mu \rightarrow \nu_\mu$, $\nu_e \rightarrow \nu_\mu$, and $\nu_\mu \rightarrow \nu_e$ transitions, the set of observable parameters is reduced considerably. In this case, the number of observable parameters is restricted to n independent mass splittings, $2n$ moduli of mixing matrix parameters, and $n-1$ CP-violating phases. Therefore, for (3+2) sterile neutrino models ($n=2$ case), for example, there are two independent mass splittings Δm_{41}^2 and Δm_{51}^2 , defined to be greater than zero, four moduli of mixing matrix parameters $|U_{e4}|$, $|U_{\mu 4}|$, $|U_{e5}|$, $|U_{\mu 5}|$, and one CP-violating phase. The convention used for the CP-phase is:

$$\phi_{45} = \arg(U_{\mu 5}^* U_{e5} U_{\mu 4} U_{e4}^*). \quad (2)$$

In that case, the general oscillation formula in Eq. 1 becomes:

$$P(\nu_\alpha \rightarrow \nu_\alpha) = 1 - 4[(1 - |U_{\alpha 4}|^2 - |U_{\alpha 5}|^2) \cdot (|U_{\alpha 4}|^2 \sin^2 x_{41} + |U_{\alpha 5}|^2 \sin^2 x_{51}) + |U_{\alpha 4}|^2 |U_{\alpha 5}|^2 \sin^2 x_{54}] \quad (3)$$

and

$$P(\nu_\alpha \rightarrow \nu_{\beta \neq \alpha}) = 4|U_{\alpha 4}|^2 |U_{\beta 4}|^2 \sin^2 x_{41} + 4|U_{\alpha 5}|^2 |U_{\beta 5}|^2 \sin^2 x_{51} + 8|U_{\alpha 5}| |U_{\beta 5}| |U_{\alpha 4}| |U_{\beta 4}| \sin x_{41} \sin x_{51} \cos(x_{54} + \phi_{45}) \quad (4)$$

The formulas for antineutrino oscillations are obtained by substituting $\phi_{45} \rightarrow -\phi_{45}$.

For the case of (3+1) sterile neutrino models ($n=1$ case), the corresponding oscillation probabilities are obtained from Eqs. 3 and 4 by setting $x_{51} = x_{54} = 0$ and $|U_{\alpha 5}| = 0$. Note that under the above assumptions, no CP violation is allowed for (3+1) models.

IV. ANALYSIS METHOD

In this section, we first provide an overview of the fitting technique. We then focus on the method followed for including the MiniBooNE datasets. The physics- and statistical-assumptions for the other null SBL experiments and LSND, which are also included in the fit, are described in detail in Ref. [5]. The constraints from atmospheric experiments, according to Ref. [19], have been incorporated as described in Ref. [15].

A. General Technique

The Monte Carlo method used to apply the oscillation formalism described in Section III closely follows the one described in Ref. [15]. We start by randomly varying sets of oscillation parameters: $\Delta m_{41}^2, |U_{e4}|, |U_{\mu 4}|$ for the case of (3+1); $\Delta m_{41}^2, |U_{e4}|, |U_{\mu 4}|, \Delta m_{51}^2, |U_{e5}|, |U_{\mu 5}|, \phi_{45}$ for the case of (3+2). Without loss of generality, we take $\Delta m_{51}^2 > \Delta m_{41}^2$. In CP-conserving models, ϕ_{45} is set to 0 or π by default, whereas in CP-violating models ϕ_{45} is allowed to vary within the full $(0, 2\pi)$ range. For each set of oscillation parameters, a signal prediction is obtained and compared to observed data for each SBL experiment, in the form of a χ^2 for each experiment. For each set of oscillation parameters that is generated, the various χ^2 's are linearly summed together to form χ_{SBL}^2 , which is then used to extract the best fit parameters and allowed regions.

A χ^2 minimization is carried out using a Markov Chain [24]. This minimization procedure relies on calculating the χ^2 difference between successive sets of parameters and using that as a measure of whether the new point in parameter space is a ‘‘good’’ point to step to, or whether a new set of parameters needs to be drawn again. This is realized in the form of a probability of accepting a new set of parameters, $P(x_i \rightarrow x_{i+1})$, given by

$$P(x_i \rightarrow x_{i+1}) = \min(1, e^{-(\chi_{i+1}^2 - \chi_i^2)/T}), \quad (5)$$

where x_i and x_{i+1} are two successive points in parameter space, and T is a Temperature parameter. Larger T values allow for larger $\Delta\chi^2$ jumps on the χ^2 surface, and therefore by varying the T value, one can avoid local minima, as well as finely scan the parameter space. This minimization method is particularly preferred in fits with large parameter space dimensionality, as in the case of (3+2) oscillation fits, due to its higher efficiency.

In extracting the various confidence level contours, we marginalize over the parameter space and report results obtained with $\Delta\chi^2$ levels corresponding to 1 degree of freedom for exclusion limits, and 2 degrees of freedom for allowed regions.

To quantify the statistical compatibility between various datasets, we use the Parameter Goodness-of-fit (PG) test introduced in [25]. In this test one quantifies how well various datasets are in agreement, by comparing the minimum χ^2 obtained by a fit where all datasets have been included as constraints to the sum of the χ^2 minima obtained by independent fits for each experiment, i.e.,

$$\chi_{PG}^2 = \chi_{min,all}^2 - \sum_i \chi_{min,i}^2, \quad (6)$$

where i runs over experimental datasets in consideration. The PG is obtained from χ_{PG}^2 based on the number of common underlying fit parameters:

$$PG = \text{prob}(\chi_{PG}^2, \text{ndf}_{PG}). \quad (7)$$

For example, for testing the compatibility between KARMEN and LSND for the (3+2) CP-conserving oscillation hypothesis, we fit for both KARMEN and LSND simultaneously to extract $\chi_{min,K+L}^2$, and for KARMEN and LSND separately to extract $\chi_{min,K}^2$, and $\chi_{min,L}^2$, respectively, and obtain:

$$\chi_{PG}^2(K, L) = \chi_{min,K+L}^2 - (\chi_{min,K}^2 + \chi_{min,L}^2). \quad (8)$$

As these are appearance experiments, there are 4 common fit parameters for a CP-conserving (3+2) model ($\Delta m_{41}^2, \Delta m_{51}^2, |U_{e4}|, |U_{\mu 4}|$, and $|U_{e5}|, |U_{\mu 5}|$); therefore,

$$PG(K, L) = \text{prob}(\chi_{PG}^2(K, L), 4). \quad (9)$$

It should be noted that χ^2 -probabilities and PG tests can lead to drastically different results [25]. This is often a consequence of a large dataset simultaneously fitted with small datasets, where the large dataset dominates the χ^2 of the simultaneous fit.

B. Inclusion of the MiniBooNE Neutrino and Antineutrino Datasets

The MiniBooNE neutrino dataset (BNB-MB(ν)), described in Sec. II, is included in the fits in the form of two side-by-side distributions of ν_e and ν_μ charged-current quasi-elastic (CCQE) events. Each distribution is a function of neutrino energy, reconstructed under the hypothesis of CCQE neutrino interaction kinematics, E_ν^{QE} . The full 200-3000 MeV range of ν_e CCQE data is used in the fit. The observed event distributions are compared to the corresponding Monte Carlo predicted distributions, and a χ^2 is calculated using a covariance matrix which includes systematic and statistical uncertainties as well as systematic correlations between the predicted ν_e and ν_μ distributions. During the fit, we vary the ν_e distribution according to the sterile neutrino oscillation parameters, but keep the ν_μ distribution unchanged. The ν_μ distribution remains unchanged during the fit, despite the possibility of ν_μ disappearance in the MiniBooNE data. We assume that including MiniBooNE ν_μ disappearance would have a small effect on sterile neutrino fit results, given the large overlap of the ν_μ disappearance limit from MiniBooNE with the corresponding limits from CDHS and CCFR84 [26]. Nevertheless, we employ this side-by-side fitting method as it takes advantage of correlations in the ν_μ and ν_e predictions and in order to effectively constrain the ν_e prediction and reduce systematic uncertainties in the $\nu_\mu \rightarrow \nu_e$ search. The fit method follows the details described in [16], except that it uses a different definition for the covariance matrix used in the χ^2 calculation. Ref. [16] involves an iterative fit method where the χ^2 calculation for each point on the parameter space being probed uses the covariance matrix calculated according to the *best-fit* signal prediction. Instead, in the MiniBooNE fits presented here, the χ^2 surface is estimated using the covariance matrix calculated according to the

signal prediction at *each point* of the parameter space under consideration. The two fit methods yield similar results, although, by definition, the iterative method of [16] results in a relative shift of the allowed region to the left, i.e. towards smaller oscillation amplitudes.

The MiniBooNE antineutrino dataset (BNB-MB($\bar{\nu}$)), described in Sec. II, is included in the fits in the same way as the BNB-MB(ν) dataset, in the form of two side-by-side E_ν^{QE} distributions of $\bar{\nu}_e$ and $\bar{\nu}_\mu$ CCQE events. In this case, the disappearance limit obtained using the MiniBooNE $\bar{\nu}_\mu$ CCQE sample provides substantial coverage of so-far unexplored sterile neutrino mass and mixing parameter space [26]. Even though we do not explicitly fit the MiniBooNE $\bar{\nu}_\mu$ CCQE distribution for disappearance, we comment on the effect of the limit from [26] in Sec. V, and justify that excluding the MiniBooNE $\bar{\nu}_\mu$ disappearance information from the fits does not substantially affect the parameter space of interest. The full 200-3000 MeV range of $\bar{\nu}_e$ CCQE data is used in the fit. The BNB-MB($\bar{\nu}$) data fit method also follows the details described in [17], except that it uses the definition for the covariance matrix described above.

In fits where both neutrino and antineutrino data are included, it has been assumed that the two datasets are fully uncorrelated. In reality, the two datasets have large systematic correlations. However, neglecting the effects of these correlations is a reasonable approximation, given that the antineutrino dataset is statistics limited.

C. Inclusion of the NuMI-beam Dataset

The NuMI-MB dataset [18], described in Sec. II, is included in the fits in the form of a distribution of ν_e CCQE events as a function of reconstructed neutrino energy, E_ν^{QE} . The predicted ν_e distribution is obtained by adding to the expected ν_e CCQE background any contribution from ν_μ to ν_e oscillations. The contribution is estimated as follows: First, a fully (100%) oscillated NuMI-MB $\nu_\mu \rightarrow \nu_e$ sample is obtained by reweighting the BNB-MB fully oscillated $\nu_\mu \rightarrow \nu_e$ Monte Carlo predicted sample according to the ratio of the NuMI-beam flux from [18] to the BNB-MB flux [20], as a function true neutrino energy. As the oscillation parameters vary during the fit, a signal prediction is calculated by rescaling the number of events in this fully oscillated sample by the corresponding oscillation probability, according to the true neutrino energy and distance travelled, from production to detection, of each event. We assume a constant L of 700 meters. The prediction is compared to the observed ν_e CCQE events as a function of 10 bins of E_ν^{QE} . The background and signal prediction are assumed to have the same fractional systematic uncertainties, and a statistical uncertainty is calculated for each point in the parameter space according to the signal prediction of each point under consideration. The data and background central value and systematic uncertainty per E_ν^{QE} bin have been estimated from [18]. Unlike the systematic

uncertainties of the BNB-MB ν_e and $\bar{\nu}_e$ CCQE datasets, the NuMI-MB ν_e CCQE systematics have not been constrained using information from the ν_μ CCQE spectrum from the NuMI beamline. Furthermore, we have not considered potential systematic correlations among the ν_e CCQE bins as a function of E_ν^{QE} .

V. (3+1) AND (3+2) MODELS AFTER THE NEW MINIBOONE ν , $\bar{\nu}$, AND NUMI RESULTS

A. (3+1) FIT RESULTS

In this section, the new MiniBooNE results are examined under a (3+1) oscillation hypothesis and compared to LSND and other null SBL experiments. The new datasets are studied first within the context of appearance-only experiments, and subsequently in fits involving both appearance and disappearance data. Fits to only antineutrino and only neutrino SBL experiments are also explored.

1. Studies with appearance-only experiments

Figure 1 shows the allowed regions obtained by independent fits to each of the following three datasets: BNB-MB(ν), BNB-MB($\bar{\nu}$), and LSND. The regions are estimated using a 2-dimensional global scan of the (3+1) parameter space ($\sin^2 2\theta_{\mu e}, \Delta m_{41}^2$). Each contour is drawn by applying a flat $\Delta\chi^2 = \chi^2(\sin^2 2\theta_{\mu e}, \Delta m_{41}^2) - \chi_{min}^2$ cut over the χ^2 surface, with respect to the global χ^2 minimum returned by the fit. The figure shows that, similarly to LSND, both BNB-MB datasets yield closed contours which exclude the no-oscillations hypothesis at 90% CL. The null χ^2 's correspond to 22.2 and 24.5 for BNB-MB(ν) and BNB-MB($\bar{\nu}$), respectively. The closed contours reflect a contradiction to the oscillation results published by the MiniBooNE collaboration; this is a consequence of the different χ^2 definition involved in the fit method used here, as pointed out in Sec. IV B. In light of these BNB-MB results and the already established LSND anomaly, we find it interesting to study sterile neutrino oscillations with the LSND, BNB-MB(ν), and BNB-MB($\bar{\nu}$) datasets assumed to be (positive) signal experiments. All three datasets yield similar best fit parameters, indicated by the stars on the three graphs, of Δm_{41}^2 of order a few eV² and $\sin^2 2\theta_{\mu e}$ of order $10^{-2} - 10^{-3}$. The minimum χ^2 and best-fit parameters returned by each experiment are summarized in Table II.

Perhaps a more interesting observation regarding Fig. 1 is the striking similarity of BNB-MB($\bar{\nu}$) and LSND 90% CL allowed regions and best-fit oscillation parameters, keeping in mind that both datasets describe antineutrino oscillations. It should be noted that in a (3+1) oscillation scenario, under the assumption of CPT invariance, there can be no difference between neutrino and antineutrino oscillation probabilities. A PG test, as described in

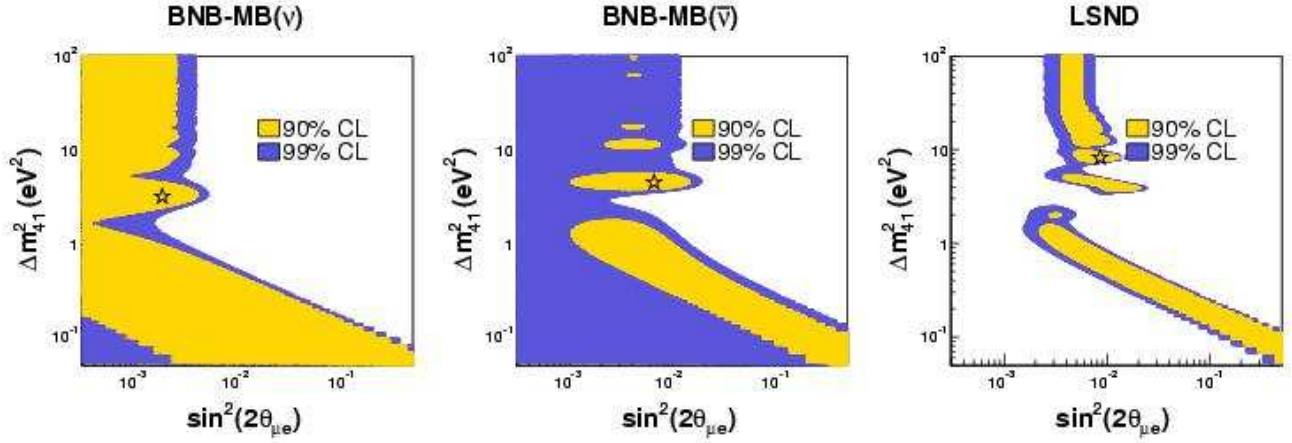


FIG. 1: Allowed regions (filled areas) at 90% and 99% CL from BNB-MB(ν)-only, BNB-MB($\bar{\nu}$)-only, and LSND-only (3+1) fits. These fits are, by construction, CP-conserving. The stars indicate the three respective best-fit points. All three datasets show closed contours at 90% CL. See text for more details.

Dataset	χ^2 (dof)	χ^2 -probability	Δm_{41}^2	$\sin^2 2\theta_{\mu e}$	$\sin^2 2\theta_{\mu\mu}$	$\sin^2 2\theta_{ee}$
Appearance-only fits:						
LSND	3.4 (3)	34%	8.19	0.0085	-	-
BNB-MB(ν)	17.5 (16)	35%	3.12	0.0018	-	-
BNB-MB($\bar{\nu}$)	17.6 (16)	35%	4.46	0.0065	-	-
NUMI-MB	2.0 (8)	98%	6.97	0.020	-	-
KARMEN	6.0 (7)	54%	6.81	0.00096	-	-
NOMAD	33.3 (28)	31%	53.3	0.00012	-	-
signal APP	50.3 (39)	11%	0.045	0.98	-	-
signal APP*	50.4 (39)	10%	0.15	0.090	-	-
null APP	46.6 (47)	49%	0.040	1.00	-	-
all APP	97.1 (88)	24%	0.045	1.00	-	-
all APP*	97.2 (88)	24%	0.15	0.090	-	-
LSND + MB-BNB($\bar{\nu}$)	22.3 (21)	38%	4.55	0.0074	-	-
LSND + MB-BNB($\bar{\nu}$)*	22.3 (21)	38%	4.55	0.0074	-	-
LSND + MB-BNB($\bar{\nu}$) + KARMEN	33.6 (30)	29%	0.57	0.0097	-	-
BNB-MB(ν) + NUMI-MB + NOMAD	57.8 (56)	40%	0.033	1.00	-	-
Appearance and disappearance fits:						
all SBL*	197.4 (196)	46%	0.92	0.0025	0.13	0.073
ν SBL	90.5 (90)	47%	0.19	0.031	0.031	0.034
$\bar{\nu}$ SBL	87.9 (103)	86%	0.91	0.0043	0.35	0.043

TABLE II: Comparison of best-fit values for mass splittings and mixing angles obtained from (3+1) fits to appearance datasets and appearance+disappearance datasets. Mass splittings are shown in eV^2 . The minimum χ^2 from each fit, as well as the χ^2 -probability are also given. The signal appearance (APP) datasets include BNB-MB(ν), BNB-MB($\bar{\nu}$) and LSND. The null APP datasets include KARMEN, NOMAD and NUMI-MB; the maximal best-fit $\sin^2 2\theta_{\mu e}$ in this case is inconsequential, as it corresponds to a best-fit Δm^2 region of very poor sensitivity. See text for more details.

*In these fits, the electron and muon content of the sterile neutrino mass eigenstate have been explicitly constrained to < 0.3 .

Sec. IV A, suggests a significantly higher compatibility (49%) between BNB-MB($\bar{\nu}$) and LSND, rather than for all three signal experiments (BNB-MB(ν), BNB-MB($\bar{\nu}$) and LSND) combined (0.26%). This is also supported by the χ^2 -probabilities returned by the fits: 11% in the

case of the BNB-MB(ν) + BNB-MB($\bar{\nu}$) + LSND fit, and 38% in the case of the BNB-MB($\bar{\nu}$) + LSND fit. This is expected, since the BNB-MB(ν) dataset prefers a mixing amplitude ~ 3 times smaller than the amplitude preferred by LSND or BNB-MB($\bar{\nu}$), and excludes the LSND and

Dataset	χ^2 -probability (%)	PG (%)
all APP	24	PG(BNB-MB(ν),BNB-MB($\bar{\nu}$),LSND,NUMI-MB,KARMEN,NOMAD) = Prob(17.3,2) = 1.7×10^{-2}
signal APP	11	PG(BNB-MB(ν),BNB-MB($\bar{\nu}$),LSND) = Prob(11.9,2) = 0.26
LSND + MB-BNB($\bar{\nu}$)	38	PG(BNB-MB($\bar{\nu}$),LSND) = Prob(1.4,2) = 49
$\bar{\nu}$ APP	29	PG(BNB-MB($\bar{\nu}$),LSND,KARMEN) = Prob(6.7,2) = 3.4
ν APP	40	PG(BNB-MB(ν),NUMI-MB,NOMAD) = Prob(4.9,2) = 8.8
all SBL*	46	PG(BNB-MB(ν),BNB-MB($\bar{\nu}$),NUMI-MB,LSND,KARMEN, NOMAD,Bugey,CHOOZ,CCFR84,CDHS,ATM) = Prob(42.0,2) = 7.6×10^{-8} PG(APP,DIS) = Prob(14.8,2) = 6.2×10^{-2} PG($\nu, \bar{\nu}$) = Prob(18.8,2) = 8.1×10^{-3}
ν SBL	47	PG(BNB-MB(ν),NUMI-MB,NOMAD,CCFR84,CDHS,ATM) = Prob(14.7,2) = 6.3×10^{-2}
$\bar{\nu}$ SBL	86	PG(BNB-MB($\bar{\nu}$),LSND,KARMEN,Bugey,CHOOZ) = Prob(8.43,2) = 1.5

TABLE III: Summary of χ^2 -probabilities for (3+1) fits with different combinations of SBL datasets, and PG results testing compatibility among different datasets. See text for more details.

* In these fits, the electron and muon content of the sterile neutrino mass eigenstate have been explicitly constrained to < 0.3 .

BNB-MB($\bar{\nu}$) best fits at 99% CL. Table III provides a summary of the above χ^2 -probabilities and PG test results.

The allowed regions obtained by a joint analysis of BNB-MB(ν) + BNB-MB($\bar{\nu}$) + LSND, as well as a joint analysis of BNB-MB($\bar{\nu}$) + LSND are shown on the left panels of Figs. 2 and 3, respectively. In the case of the combined fit of all three datasets (Fig. 2), due to the difference in preferred mixing amplitudes mentioned in the previous paragraph, the best-fit point ends up shifting from an intermediate Δm^2 and small mixing amplitude to a smaller Δm^2 and maximal mixing amplitude of 0.98. Obviously a maximal mixing amplitude is unphysical in the case of sterile neutrino oscillations. If the fits are repeated with the electron and muon content of the sterile mass eigenstate limited to values less than 0.3 [34], the returned χ^2 -probabilities are 10% and 38%, for BNB-MB(ν) + BNB-MB($\bar{\nu}$) + LSND and BNB-MB($\bar{\nu}$) + LSND, respectively; the reduction in $\sin^2 2\theta_{\mu e}$ space has essentially no effect on these results. The best-fit parameters from these fits are also given in Table II.

Figures 2 and 3 also illustrate the limits from various combinations of the remaining three (null) SBL appearance experiments (KARMEN, NOMAD, and NUMI-MB) under a (3+1) oscillation scenario, overlaid on the allowed regions described above.

The 90% and 99% CL limits obtained by each of the null appearance experiments, NUMI-MB, KARMEN, and NOMAD are shown on the left panel of Fig. 2. These limits correspond to the upper $\sin^2 2\theta_{\mu e}$ values allowed at each Δm^2_{41} , estimated using a one-sided raster scan of the parameter space. It is interesting to point out that, despite the indication of a slight excess (1.2σ) of observed ν_e -like events for neutrino energies below 900 MeV found in the NuMI analysis [18], the currently assumed NUMI-MB systematic and statistical uncertainties are quite large, resulting in a limit that is much weaker relative to the limits of KARMEN and NOMAD. In fact, due to this excess and the large systematic uncertainties, the NUMI-MB dataset provides a very good fit to

(3+1) models, with a χ^2 -probability of 98%. Additional data and reduced systematic uncertainties in the NUMI-MB analysis are necessary for higher sensitivity and more conclusive results. This is currently an ongoing joint effort and new results are expected soon. The limits from a combined NUMI-MB + KARMEN + NOMAD analysis are shown on the middle panel of Fig. 2. Both panels illustrate that the null appearance experiments provide essentially no constraints to the parameter space allowed by the BNB-MB and LSND datasets.

Table II further illustrates that the best-fit parameters obtained independently from the NUMI-MB and KARMEN datasets are similar to those of LSND, BNB-MB(ν), and BNB-MB($\bar{\nu}$). The NOMAD dataset, on the other hand, prefers a much larger $\Delta m^2_{41} \sim 50\text{eV}^2$, and a much smaller $\sin^2 2\theta_{\mu e} \sim 10^{-4}$.

A combined analysis of all appearance data yields a χ^2 -probability of 24% for the best fit hypothesis, both in the case where maximal mixing is allowed, and in the case where the electron and muon content of the sterile mass eigenstate has been limited to small values (< 0.3). The allowed region obtained by a joint analysis of all appearance experiments under a (3+1) oscillation scenario is shown in the right panel of Fig. 2.

Similarly, Fig. 3 (left) corresponds to the allowed region obtained by a joint analysis of BNB-MB($\bar{\nu}$) + LSND. The limit shown is that of the KARMEN experiment, which is the only other SBL experiment to perform an appearance search with antineutrinos. The KARMEN limit provides substantial coverage of the joint LSND and BNB-MB($\bar{\nu}$) allowed region, excluding the best-fit point of the LSND + BNB-MB($\bar{\nu}$) fit at $> 99\%$ CL. However, KARMEN imposes little constraint to the lower- Δm^2 allowed solutions. A joint analysis of all three datasets yields a χ^2 -probability of 29% for the best fit hypothesis, and an allowed region shown on the right panel of Fig. 3. The χ^2 -probability remains the same for fits where the electron and muon content of the sterile mass eigenstates have been limited to values less than 0.3. Nevertheless, as shown in Table III, the three datasets are compatible

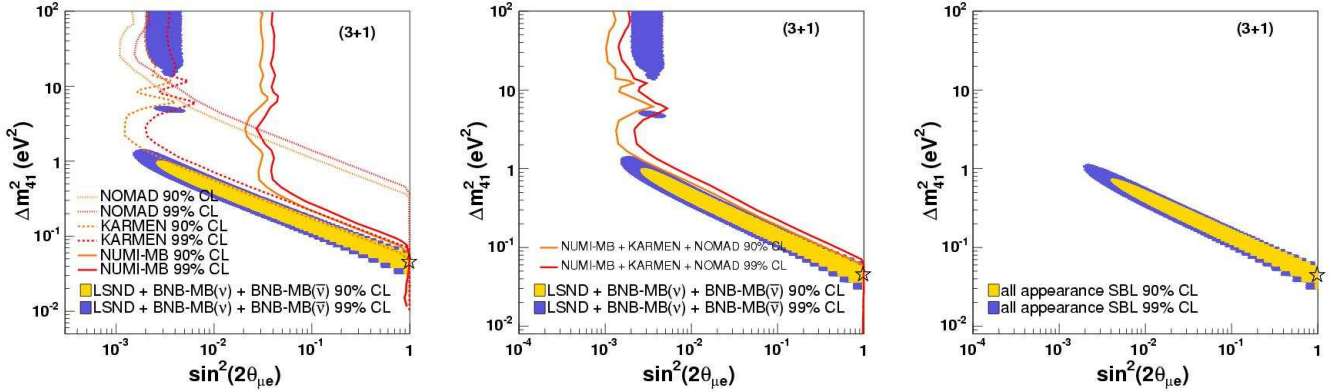


FIG. 2: Left: Allowed 90% and 99% CL regions (light and dark filled areas, respectively) from a combined analysis of BNB-MB(ν), BNB-MB($\bar{\nu}$) and LSND datasets, and 90% and 99% exclusion limits (light and dark curves, respectively) from each of the null appearance experiments, NUMI-MB (solid curves), KARMEN (dashed curves) and NOMAD (dotted curves). Middle: The same allowed region with overlaid 90% and 99% exclusion limits from a combined analysis of all null appearance experiments. Right: Allowed region obtained by a combined analysis of all appearance datasets, signal and null. See text for more details.

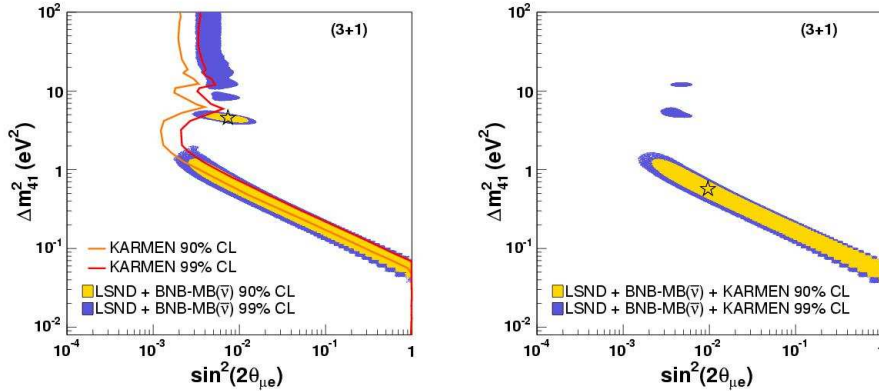


FIG. 3: Left: The allowed 90% and 99% CL regions (light and dark filled areas, respectively) from a combined analysis of BNB-MB($\bar{\nu}$) and LSND datasets, and 90% and 99% exclusion limits (light and dark curves, respectively) from KARMEN. A comparison of only these three experiments is interesting, as these three experiments have searched for antineutrino oscillations at short baselines. Right: The allowed regions obtained from a combined analysis of all three experiments (BNB-MB($\bar{\nu}$), LSND, and KARMEN). See text for more details.

at only 3.4%. New results from MiniBooNE with increased antineutrino statistics should be able to provide more information to these fits [17].

2. Studies with appearance and disappearance experiments

Much stronger constraints than those of the null appearance experiments are provided by the null disappearance experiments (CCFR84, CDHS, CHOOZ, and Bugey) and atmospheric constraints, under the assump-

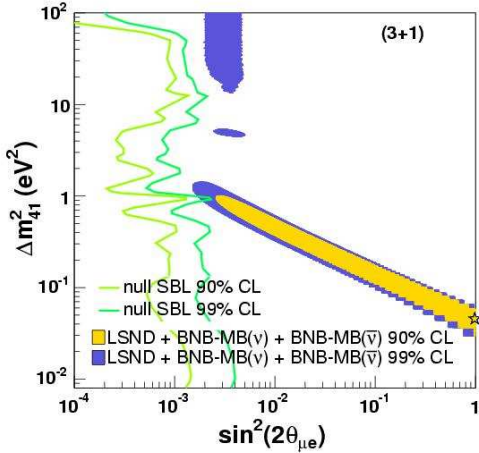


FIG. 4: The allowed 90% and 99% CL regions (light and dark filled areas, respectively) from a combined analysis of BNB-MB(ν) + BNB-MB($\bar{\nu}$) + LSND datasets, and 90% and 99% exclusion limits (light and dark curves, respectively) from a combined analysis of all remaining (null, appearance and disappearance) SBL experiments. The null fit includes atmospheric constraints. The null SBL experiments exclude the joint 99% CL allowed region at 99% CL.

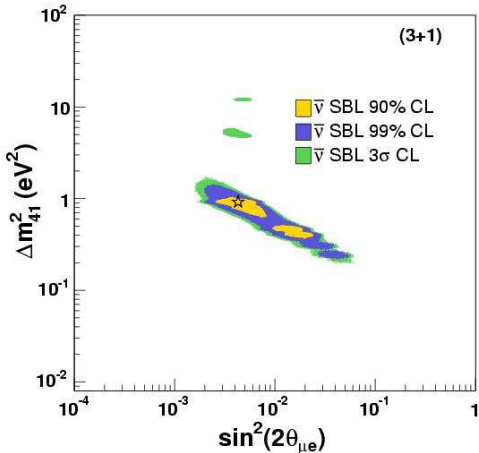


FIG. 5: The allowed 90%, 99%, and 3σ CL regions from a combined analysis of all antineutrino SBL datasets. See text for more details.

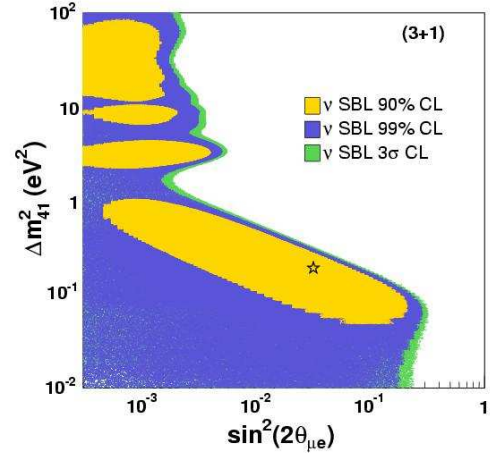


FIG. 6: The allowed 90%, 99%, and 3σ CL regions from a combined analysis of all neutrino SBL datasets. See text for more details.

tions of CPT conservation and unitarity of the neutrino mixing matrix. The 90% and 99% CL exclusion limits from a combined analysis of all remaining (null) experiments (NUMI-MB, KARMEN, NOMAD, Bugey, CHOOZ, CCFR84, CDHS, and atmospheric constraints) are shown in Fig. 4. The figure shows that the parameter space jointly-allowed by BNB-MB(ν) + BNB-MB($\bar{\nu}$) + and LSND at 99% CL is excluded by a combined analysis of all null SBL experiments, appearance and disappearance, at 99% CL. The severe tension between LSND and the null SBL experiments [14] continues to exist and in fact increases further with the addition of BNB-MB(ν) and BNB-MB($\bar{\nu}$) data. The signal results show low (0.15%) compatibility with null results. The LSND result remains to be mostly responsible for the low compatibility, as the BNB-MB(ν) and BNB-MB($\bar{\nu}$) experiments show 14% and 3.7% compatibility with the null experiments, respectively.

Figure 5 shows the allowed region obtained by the joint BNB-MB($\bar{\nu}$) + LSND + KARMEN + Bugey + CHOOZ analysis. Here, the $\bar{\nu}_e$ disappearance constraints from Bugey and CHOOZ are interesting to consider from the perspective of a joint analysis of only antineutrino SBL experiments. In a joint fit, all antineutrino SBL experiments yield a high χ^2 -probability of 86%, and 1.5% compatibility. In these fits, Bugey and CHOOZ constrain $|U_{e4}|$, but provide no direct constraints on $|U_{\mu 4}|$. However, a joint analysis with the LSND, BNB-MB($\bar{\nu}$), and KARMEN appearance experiments, which are sensitive to the product of $|U_{e4}||U_{\mu 4}|$, provides indirect constraints to the $|U_{\mu 4}|$ mixing element. Current constraints from MiniBooNE on $\bar{\nu}_\mu$ disappearance [26] are able to constrain $\sin^2 2\theta$ values for $\sim 1 < \Delta m^2 < 10$ eV 2 , and would therefore provide little constraint on the parameter space of Fig. 5. However, new results from a joint MiniBooNE

and SciBooNE [27] $\bar{\nu}_\mu$ disappearance search, which are expected soon [28], may be able to probe this region, and will be interesting within the context of CPT-violating models. According to the best-fit oscillation parameters from a fit to only antineutrino SBL data, MiniBooNE should observe muon antineutrino disappearance with an amplitude of $\sin^2 2\theta_{\mu\mu} \sim 0.35$, at $\Delta m^2 \sim 0.91 \text{ eV}^2$. The MINOS experiment [29] should also have sensitivity to these oscillation parameters in antineutrino running mode; muon antineutrino disappearance search results from MINOS are expected soon [30]. Incorporation of the upcoming MiniBooNE and MINOS disappearance results in these fits is currently being investigated.

Neutrino-only fits also yield a reasonably high χ^2 -probability of 47%; the corresponding allowed regions are shown in Fig. 6. Interestingly, fits to only neutrino SBL data also yield a closed contour at 90% CL. The parameter space, however, points to smaller mixing amplitudes relative to those preferred by the antineutrino-only fit. Neutrino-only fits and antineutrino-only fits are incompatible, with a PG of 8.1×10^{-5} , as shown in Table III. The large incompatibility of antineutrino and neutrino SBL results suggests that the neutrino and antineutrino datasets cannot be accommodated within a (3+1) CPT-conserving sterile neutrino oscillation scenario. However, the constraining power of antineutrino SBL experiments alone on Δm_{41}^2 and $\sin^2 2\theta_{\mu e}$ is remarkable, and invites exploration of models that provide the possibility of different oscillation patterns for neutrinos versus antineutrinos.

The best-fit parameters from neutrino-only and antineutrino-only fits are summarized in Table II. The best-fit results from the (3+1) oscillation fit involving all SBL datasets are also shown.

B. (3+2) FIT RESULTS

Neutrino oscillation models with more than one sterile neutrino have been of particular interest because they open up the possibility of observable CP violation effects in short-baseline neutrino oscillations. If (3+n) sterile neutrino oscillations are realized in nature, with $n > 1$, CP violation becomes a natural possibility, which is very appealing from the perspective of theories attempting to explain the matter-antimatter asymmetry in our universe [31].

In this section, the new MiniBooNE results are examined under both a CP-conserving (CPC) and a CP-violating (CPV) (3+2) oscillation hypothesis. The new results are studied first within the context of appearance-only experiments, and subsequently in fits involving both appearance and disappearance data.

From the point of view of the data at hand from LSND, BNB-MB(ν), and BNB-MB($\bar{\nu}$) (see Fig. 1), CP violation offers the potential of reconciling two experimental signatures—an excess at LSND at 3.8σ significance and one suggested at 90% CL in BNB-MB antineutrino data,

both pointing to relatively large mixing, with a possible excess found in BNB-MB neutrino data suggesting relatively small mixing, both at a similar L/E —as manifestations of the same underlying oscillation hypothesis.

It should be noted that in the studies presented in this section, due to the larger dimensionality of the fits, the electron and muon content of the sterile mass eigenstates have been limited to values less than 0.3. This is a realistic assumption for sterile neutrino oscillation models.

1. Studies with appearance-only experiments

Allowing for CP violation in (3+2) fits to LSND and BNB-MB(ν and $\bar{\nu}$) data leads to a reduction in absolute χ^2 of 4.4, for 1 degree of freedom (dof), corresponding to a best-fit CPV phase $\phi_{45} = 1.7\pi$. The χ^2 -probability of the fit increases from 13% in the CPC case to 21% in the CPV case. The same test can be performed using all appearance data. In this case, allowing for CP violation leads to a reduction in χ^2 of 3.2 for 1 dof, with a best-fit CPV phase $\phi_{45} = 1.1\pi$. The χ^2 -probability from the CPV fit is comparable to that of a signal-only fit, at 27%.

The 90% and 99% CL allowed ($\Delta m_{41}^2, \Delta m_{51}^2$) parameter space obtained by a combined fit to BNB-MB(ν) + BNB-MB($\bar{\nu}$) + LSND is shown in Fig. 7. The figure illustrates that both scenarios, CPC (left) and CPV (right), prefer similar Δm^2 parameters at 99% CL; however, the CPV hypothesis is more restrictive in Δm_{51}^2 at 90% CL, shown by the shrunk light yellow (light grey) area in the right plot.

A similar 99% CL allowed parameter space is obtained when data from all appearance experiments are included in the fits, shown in Fig. 8. Here, the effect of CP violation on constraining Δm_{51}^2 is not as strong.

The best-fit parameters for the signal-only and appearance-only fits are summarized in Table IV.

2. Studies with appearance and disappearance experiments

A dramatic reduction in the allowed ($\Delta m_{41}^2, \Delta m_{51}^2$) parameter space occurs once all SBL datasets are considered in the fit, as shown in Fig. 9. Compared to the CPC hypothesis, the CPV hypothesis fails to provide a substantially better description of the data, reflected by the reduction in χ^2 of 1.3 for 1 dof. The returned χ^2 -probability for both CPC and CPV fits is 52%; however, a PG test among all experimental datasets yields incompatibility between all datasets at more than 5σ significance. This large incompatibility in part reflects the large number of datasets being compared, a consequence of the nature of the PG test; however, as discussed in Sec. VI, an underlying source of tension exists and is due to three particular datasets: BNB-MB(ν), CDHS, and atmospheric constraints. The best fit parameters extracted from a fit to all SBL data are also summarized in Table IV.

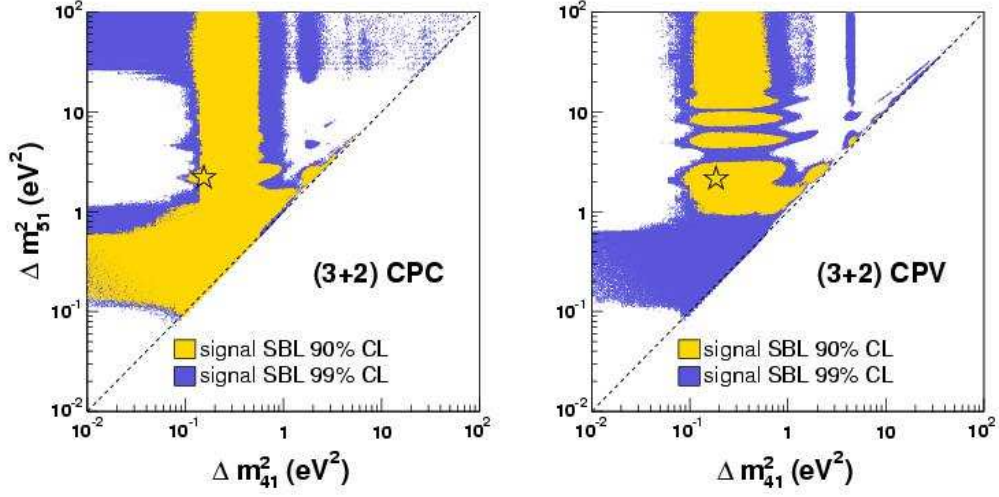


FIG. 7: Allowed regions in $(\Delta m_{41}^2, \Delta m_{51}^2)$ space for fits to CP-conserving (CPC, left) and CP-violating (CPV, right) (3+2) oscillation models. Only the BNB-MB(ν), BNB-MB($\bar{\nu}$) and LSND datasets have been included in the fit.

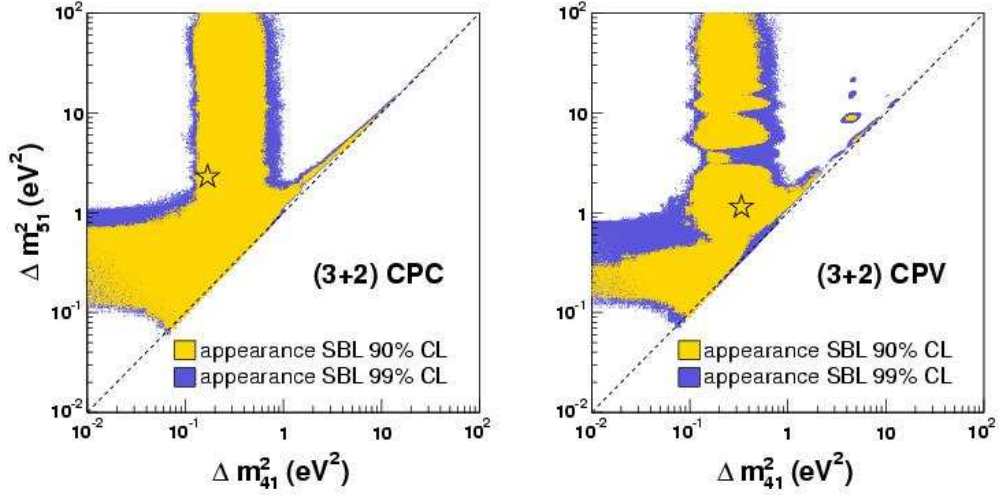


FIG. 8: Allowed regions in $(\Delta m_{41}^2, \Delta m_{51}^2)$ space for fits to CP-conserving (CPC, left) and CP-violating (CPV, right) (3+2) oscillation models. Only appearance datasets have been included in the fit.

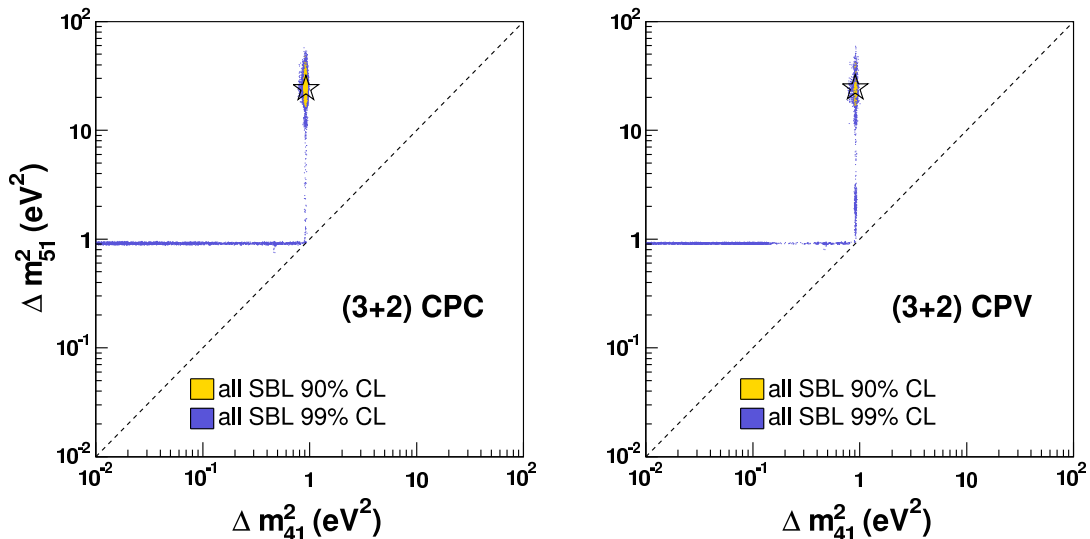


FIG. 9: Allowed regions in $(\Delta m_{41}^2, \Delta m_{51}^2)$ space for fits to CP-conserving (CPC, left) and CP-violating (CPV, right) (3+2) oscillation models. All SBL datasets (appearance and disappearance) and atmospheric constraints have been included in the fit.

A comparison of Tables II and IV suggests that, with the addition of the new datasets from MiniBooNE, the (3+2) oscillation hypothesis now provides only a marginally better description of all data, compared to the (3+1) hypothesis. Compared to (3+1) models, (3+2) CP-conserving models give a reduction of 5.9 χ^2 units for 3 additional fit parameters, while (3+2) CP-violating models give a reduction of 7.2 χ^2 units with 4 additional parameters. This represents a relative improvement that is significantly smaller than that found in Ref. [5] from fits using datasets prior to the new MiniBooNE results.

Figure 10 shows the projection of $\Delta\chi^2 = \chi^2 - \chi_{min}^2$ as a function of the CP-violating phase ϕ_{45} for the three fits discussed in this section: the appearance-only projection is shown in the solid orange (light grey) line, the BNB-MB(ν) + BNB-MB($\bar{\nu}$) + LSND projection in dashed orange (light grey), and the fit with all SBL experiments is shown in blue (dark grey). Despite the fact that the signal experiments yield a best-fit ϕ_{45} of 1.1π , all three (3+2) CPV fits favor a similar phase range around $\phi_{45} \sim 1.7\pi$, as illustrated by the three overlapping dips in the $\Delta\chi^2$ distribution.

VI. CONSTRAINTS TO (3+2) CP-VIOLATING FITS FROM EACH SBL EXPERIMENT

In this section we study the constraints to experimentally allowed (3+2) CP-violating oscillations by each of the SBL experiments. This is accomplished through a study where fits are performed using all-but-one experiment at a time. Within this study, we are also interested in examining the source of incompatibility between ap-

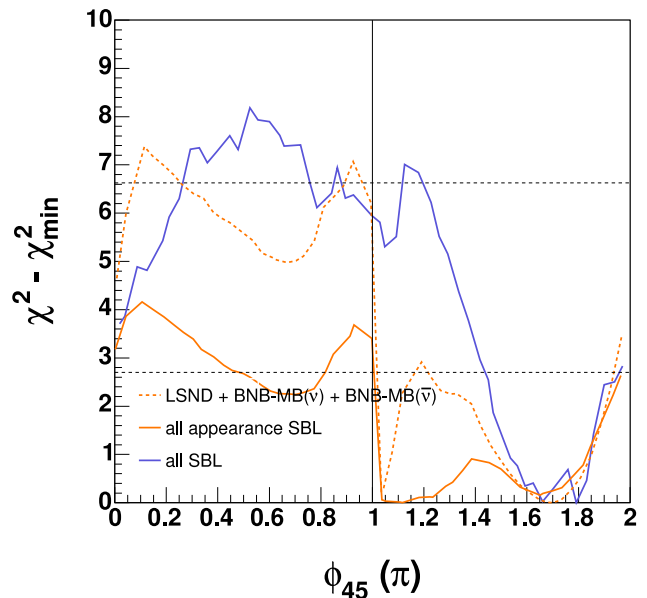


FIG. 10: Projection of $\Delta\chi^2 = \chi^2 - \chi_{min}^2$ as a function of the CP-violating phase ϕ_{45} . The dashed horizontal lines indicate the 90% and 99% CL $\Delta\chi^2$.

pearance and disappearance data, as well as testing compatibility between neutrino and antineutrino appearance search results within a CP-violating scenario. The latter is motivated by the larger incompatibility found in neutrino versus antineutrino fits, as opposed to appearance

Dataset	Fit	χ^2 (dof)	χ^2 -probability	Δm_{41}^2	Δm_{51}^2	$ U_{e4} $	$ U_{\mu 4} $	$ U_{e5} $	$ U_{\mu 5} $	ϕ_{45}
signal APP	CPV	42.5(36)	21%	0.14	2.06	0.35	0.40	0.056	0.18	1.7π
signal APP	CPC	46.9(37)	13%	2.01	2.22	0.42	0.24	0.33	0.33	0
all APP	CPV	92.6(85)	27%	0.28	1.12	0.44	0.20	0.21	0.094	1.1π
all APP	CPC	95.8(86)	22%	0.18	2.31	0.32	0.38	0.086	0.071	0
all SBL	CPV	190.2(192)	52%	0.90	24.5	0.12	0.14	0.065	0.18	1.8π
all SBL	CPC	191.5(193)	52%	0.92	24.0	0.12	0.14	0.070	0.14	0

TABLE IV: Comparison of best-fit values for mass splittings and mixing parameters for (3+2) CP-conserving (CPC) and CP-violating (CPV) models. Mass splittings are shown in eV^2 . The appearance experiments include BNB-MB(ν and $\bar{\nu}$), LSND, NUMI-MB, KARMEN, and NOMAD. The signal experiments include LSND, BNB-MB(ν), and BNB-MB($\bar{\nu}$). See text for more details.

versus disappearance fits.

Table V summarizes the χ^2 -probability and PG results from (3+2) CP-violating fits. The upper rows summarize χ^2 -probabilities and PG's from fits to all SBL experiments, as well as fits to appearance-only, disappearance-only, neutrino-only, antineutrino-only, neutrino appearance-only, and antineutrino appearance-only datasets. Appearance and disappearance datasets, as well as neutrino and antineutrino datasets are incompatible at 3.0σ or higher. Grouping SBL appearance-only datasets according to whether they are neutrino or antineutrino experiments yields higher compatibilities—56% among $\bar{\nu}$ appearance experiments, and 18% among ν appearance experiments. However, the compatibility between ν and $\bar{\nu}$ appearance-only results is still low, at 2.2%. In the case where disappearance experiments are included in the comparison between neutrino and antineutrino fits, the compatibility of all $\bar{\nu}$ SBL datasets remains reasonable, at 5.8%, but the compatibility among all ν SBL datasets, and the compatibility between $\bar{\nu}$ and ν results are both $<1\%$.

The remaining rows of Table V provide the χ^2 -probabilities of global fits under the same oscillation scenario where one experiment is excluded from the fit at a time (as indicated by the “-” sign in the table). The χ^2 probabilities of all fits are acceptable, ranging between 25.7% for a fit excluding the Bugey dataset, and 70.6% for a fit excluding the LSND dataset. Aside from LSND, three experiments stand out as having poorest compatibility when compared to a global fit with all other SBL datasets: 1) BNB-MB(ν), 2) CDHS and 3) atmospheric constraints (ATM). These three experiments have been identified as the possible source of tension among appearance and disappearance experiments. The remaining combinations yield reasonably high compatibility of at least 45%, with the exception of LSND and BNB-MB($\bar{\nu}$) which are compatible with the remaining datasets at 2.9% and 20%, respectively.

To further test the hypothesis that the tension between appearance and disappearance experiments is a result of the BNB-MB(ν) and CDHS datasets and atmospheric constraints, the compatibility between appearance and disappearance experiments is re-evaluated several times. Each time, a different combination of these three exper-

iments is excluded from the fits. The results are summarized in Table VI. The compatibility among appearance and disappearance experiments with BNB-MB(ν), CDHS, and atmospheric constraints excluded from the fits is high, at 36.4%. The BNB-MB(ν) dataset alone is not responsible for the disagreement between appearance and disappearance experiments, as suggested by the sixth row of the Table VI. Even with BNB-MB(ν) included in the fit, a compatibility of 15.7% can be obtained if CDHS and atmospheric constraints are excluded from the fit. Instead, the tension seems to exist mainly between BNB-MB(ν) and CDHS, and BNB-MB(ν) and atmospheric constraints.

The same test can be performed between neutrino and antineutrino experiments. The results are summarized in Table VII. Again, the compatibility between neutrino and antineutrino experiments is re-evaluated several times; each time, a different combination of the BNB-MB(ν), CDHS, and atmospheric constraint datasets is excluded from the fits. Here, the compatibility among neutrino and antineutrino experiments with BNB-MB(ν), CDHS, and atmospheric constraints excluded from the fits is even higher, at 44.0%. In this case, however, the BNB-MB(ν) dataset is just as responsible for the disagreement between neutrino and antineutrino experiments as the CDHS dataset and atmospheric constraints alone. The tension seems to be caused by all three experiments.

It is possible that higher compatibility between BNB-MB(ν) and all remaining SBL datasets may be achieved if the fits are to be repeated with the low energy region ($200 < E_\nu^{QE} < 475$ MeV) excluded from the BNB-MB(ν) dataset.

A global analysis with BNB-MB(ν), CDHS, and atmospheric constraints excluded from the fit yields a χ^2 -probability of 83% but still relatively low compatibility, of 0.4%.

VII. CONCLUSIONS

We have re-examined global fits to sterile neutrino oscillation models, using new data from MiniBooNE. Those include the final MiniBooNE neutrino mode results and

Dataset	χ^2 (<i>dof</i>)	χ^2 -probability (%)	PG (%)
all SBL	190.2 (192)	52.3	PG(BNB-MB(ν),BNB-MB($\bar{\nu}$),NUMI-MB,LSND,KARMEN, NOMAD,Bugey,CHOOZ,CCFR84,CDHS,ATM) = Prob(49.1,5) = 2.2×10^{-7} PG(APP,DIS) = Prob(16.3,4) = 0.26 PG($\nu, \bar{\nu}$) = Prob(21.0,5) = 8.2×10^{-2}
all APP	92.6 (85)	26.9	PG(BNB-MB(ν),BNB-MB($\bar{\nu}$),NUMI-MB,LSND,KARMEN, NOMAD) = Prob(24.6,5) = 1.7×10^{-2}
all DIS	81.3 (103)	94.4	PG(Bugey,CHOOZ,CCFR84,CDHS,ATM) = Prob(8.14,4) = 8.6
all ν	86.1 (86)	47.8	PG(BNB-MB(ν),NUMI-MB,NOMAD,CCFR84,CDHS,ATM) = Prob(17.4,5) = 0.37
all $\bar{\nu}$	83.2 (99)	87.3	PG(BNB-MB($\bar{\nu}$),KARMEN,LSND,Bugey,CHOOZ) = Prob(10.7,5) = 5.8
ν APP	50.6 (53)	56.8	PG(BNB-MB(ν),NUMI-MB,NOMAD) = Prob(3.91,5) = 56
$\bar{\nu}$ APP	28.9 (27)	36.7	PG(BNB-MB($\bar{\nu}$),KARMEN,LSND) = Prob(7.55,5) = 18 PG(ν APP, $\bar{\nu}$ APP) = Prob(13.1,5) = 2.2
all - BNB-MB(ν)	167.2 (174)	63.2	PG(all SBL - BNB-MB(ν) , BNB-MB(ν)) = Prob(12.1,5) = 3.4
all - BNB-MB($\bar{\nu}$)	168.5 (174)	60.3	PG(all SBL - BNB-MB($\bar{\nu}$) , BNB-MB($\bar{\nu}$)) = Prob(7.34,5) = 20
all - NUMI-MB	184.2 (182)	43.9	PG(all SBL - NUMI-MB , NUMI-MB) = Prob(4.34,5) = 50
all - LSND	176.1 (187)	70.6	PG(all SBL - LSND , LSND) = Prob(12.5,5) = 2.9
all - KARMEN	180.2 (183)	54.6	PG(all SBL - KARMEN , KARMEN) = Prob(4.72,5) = 45
all - NOMAD	154.2 (162)	65.6	PG(all SBL - NOMAD , NOMAD) = Prob(1.89,5) = 86
all - Bugey	142.2 (132)	25.7	PG(all SBL - Bugey , Bugey) = Prob(3.07,4) = 55
all - CHOOZ	180.9 (178)	42.6	PG(all SBL - CHOOZ , CHOOZ) = Prob(3.06,4) = 55
all - CCFR84	174.7 (174)	47.0	PG(all SBL - CCFR84 , CCFR84) = Prob(0.82,4) = 94
all - CDHS	175.4 (177)	51.9	PG(all SBL - CDHS , CDHS) = Prob(7.48,4) = 11
all - ATM	184.4 (190)	60.0	PG(all SBL - ATM , ATM) = Prob(5.78,2) = 5.6

TABLE V: Comparison of χ^2 -probabilities for (3+2) CP-violating fits with different combinations of SBL datasets. Also shown are PG results testing compatibility among different datasets. The last eleven rows of the table provide the compatibility (PG) between the experiment being removed from each fit and all remaining experiments. See text for more details.

Datasets	PG (%)
APP vs. DIS	0.26
APP (no BNB-MB(ν) vs. DIS (no CDHS + ATM)	36.4
APP (no BNB-MB(ν) vs. DIS (no CDHS)	0.58
APP (no BNB-MB(ν) vs. DIS (no ATM)	0.82
APP (no BNB-MB(ν) vs. DIS	0.10
APP vs. DIS (no CDHS + ATM)	15.7
APP vs. DIS (no CDHS)	0.76
APP vs. DIS (no ATM)	1.4

TABLE VI: Comparison of compatibility between appearance (APP) and disappearance (DIS) experiments, within a (3+2) CP-violating scenario. The BNB-MB(ν) dataset, CDHS dataset, and atmospheric constraints (ATM) are removed from the fits as specified in order to establish the source of tension between appearance and disappearance experiments. See text for more details.

the first, low statistics MiniBooNE antineutrino results, as well as first results from the off-axis NuMI beam observed in the MiniBooNE detector.

Within a (3+1) CP- and CPT-conserving scenario, we have found that the dataset collected by MiniBooNE using the NuMI off-axis beam (NUMI-MB) currently provides very weak constraints to sterile neutrino fits, due to large systematic uncertainties. Updated NuMI results, expected soon, should have a greater impact on these fits. Within the same oscillation framework, the MiniBooNE

Datasets	PG (%)
ν vs. $\bar{\nu}$	8.2×10^{-2}
ν (no BNB-MB(ν) + CDHS + ATM) vs. $\bar{\nu}$	44.0
ν (no BNB-MB(ν) + CDHS) vs. $\bar{\nu}$	1.6
ν (no BNB-MB(ν) + ATM) vs. $\bar{\nu}$	1.8
ν (no BNB-MB(ν) vs. $\bar{\nu}$	0.36
ν (no CDHS + ATM) vs. $\bar{\nu}$	0.70
ν (no CDHS) vs. $\bar{\nu}$	0.68
ν (no ATM) vs. $\bar{\nu}$	0.36

TABLE VII: Comparison of compatibility between neutrino (ν) and antineutrino ($\bar{\nu}$) experiments, within a (3+2) CP-violating scenario. The BNB-MB(ν) dataset, CDHS dataset, and atmospheric constraints (ATM) are removed from the fits as specified in order to establish the source of tension between neutrino and antineutrino experiments. See text for more details.

antineutrino dataset (BNB-MB($\bar{\nu}$)) is found in agreement with LSND, yielding, in a combined analysis with LSND and KARMEN under a (3+1) oscillation hypothesis, a χ^2 -probability of 29%, and best-fit parameters similar to those of LSND. Updated MiniBooNE antineutrino appearance results, with almost twice the current statistics are expected in the near future. The MiniBooNE neutrino dataset (BNB-MB(ν)), although suggestive of an excess that could be described by a (3+1) oscillation hypothesis with a χ^2 probability of 35%, is found incompat-

ible with the signals from the MiniBooNE antineutrino and LSND results. The remaining null appearance and disappearance experiments (NUMI-MB(ν), KARMEN, NOMAD, Bugey, CHOOZ, CDHS, CCFR84) and atmospheric oscillation data impose strong constraints to the parameter space allowed by a combined analysis of MiniBooNE neutrino and antineutrino and LSND data, excluding the 99% CL allowed region at 99% CL. However, the constraints from antineutrino disappearance experiments on the parameter space allowed by antineutrino appearance experiments (BNB-MB($\bar{\nu}$), LSND, and KARMEN) are weaker. All antineutrino experiments yield a best-fit χ^2 -probability of 86%, and exclude the no-oscillations hypothesis at $>5.0\sigma$. The best-fit parameters are similar to those of LSND, and correspond to a muon antineutrino disappearance amplitude of 0.35, which may be addressed by upcoming results from MiniBooNE and MINOS on muon antineutrino disappearance. Additionally, fits to all neutrino experiments yield a best-fit χ^2 -probability of 47% and exclude the null hypothesis at $>90\%$ CL.

Furthermore, we find that with the addition of the new MiniBooNE datasets, the (3+2) oscillation models provide only a marginally better description of all SBL datasets compared to (3+1) models. In the case of (3+2) fits, CP violation only allows for a small improvement in χ^2 -probability for fits to only BNB-MB(ν) + BNB-MB($\bar{\nu}$) + LSND, and fits to only appearance experiments. In the case of global fits, the χ^2 -probability for the best fit hypothesis is 52%. The best fit corresponds

to large but not maximal CP violation ($\phi_{45} = 1.8\pi$). The high incompatibility ($>3.0\sigma$) among appearance and disappearance data remains after the addition of the new MiniBooNE results. This incompatibility is a result of the BNB-MB(ν) and CDHS datasets and atmospheric constraints. The compatibility between appearance and disappearance data with these three experiments excluded from the fits is significantly higher, at 36%.

Neutrino and antineutrino datasets are also incompatible within a (3+2) CP-violating scenario, at the level of $>3.0\sigma$. The compatibility improves slightly to 2.2% in the case of comparing appearance-only neutrino and antineutrino datasets.

Overall, allowing for mixing with multiple sterile neutrino states or CP violation does not seem sufficient to allow incorporating all SBL experiments within a CPT-conserving, sterile neutrino oscillation framework. It may be that there is an issue with one or more of the three datasets: BNB-MB(ν), including the low-energy excess, CDHS, or atmospheric constraints; alternatively, theories with CPT-violating oscillations or effective CPT violation [32, 33] may succeed in reconciling all short-baseline oscillation signatures, and should be explored.

Acknowledgments

We thank Bill Louis for valuable discussions. We also thank the National Science Foundation for their support.

-
- [1] C. Athanassopoulos *et al.* [LSND Collaboration], Phys. Rev. Lett. **77**, 3082 (1996) [arXiv:nucl-ex/9605003]; C. Athanassopoulos *et al.* [LSND Collaboration], Phys. Rev. C **58**, 2489 (1998) [arXiv:nucl-ex/9706006]; A. Aguilar *et al.* [LSND Collaboration], Phys. Rev. D **64**, 112007 (2001) [arXiv:hep-ex/0104049].
 - [2] O. L. G. Peres and A. Y. Smirnov, Nucl. Phys. B **599**, 3 (2001) [arXiv:hep-ph/0011054].
 - [3] A. Strumia, Phys. Lett. B **539**, 91 (2002) [arXiv:hep-ph/0201134].
 - [4] W. Grimus and T. Schwetz, Eur. Phys. J. C **20**, 1 (2001) [arXiv:hep-ph/0102252].
 - [5] M. Sorel, J. M. Conrad and M. H. Shaevitz, Phys. Rev. D **70**, 073004 (2004) [arXiv:hep-ph/0305255].
 - [6] M. Maltoni, T. Schwetz, M. A. Tortola and J. W. F. Valle, Nucl. Phys. B **643**, 321 (2002) [arXiv:hep-ph/0207157].
 - [7] B. Armbruster *et al.* [KARMEN Collaboration], Phys. Rev. D **65**, 112001 (2002) [arXiv:hep-ex/0203021].
 - [8] P. Astier *et al.* [NOMAD Collaboration], Phys. Lett. B **570**, 19 (2003) [arXiv:hep-ex/0306037]; D. Gibin, Nucl. Phys. Proc. Suppl. **66**, 366 (1998); V. Valuev [NOMAD Collaboration], SPIRES entry *Prepared for International Europhysics Conference on High-Energy Physics (HEP 2001), Budapest, Hungary, 12-18 Jul 2001*
 - [9] Y. Declais *et al.*, Nucl. Phys. B **434**, 503 (1995).
 - [10] M. Apollonio *et al.*, [arXiv:hep-ex/0301017].
 - [11] I. E. Stockdale *et al.*, Phys. Rev. Lett. **52**, 1384 (1984).
 - [12] F. Dydak *et al.*, Phys. Lett. B **134**, 281 (1984).
 - [13] A. A. Aguilar-Arevalo *et al.* [The MiniBooNE Collaboration], Phys. Rev. Lett. **98**, 231801 (2007) [arXiv:hep-ex/0704.1500].
 - [14] M. Maltoni and T. Schwetz, Phys. Rev. D **76**, 093005 (2007) [arXiv:hep-ph/0705.0107].
 - [15] G. Karagiorgi *et al.*, Phys. Rev. D **75**, 013011 (2007) [arXiv:hep-ph/0609177].
 - [16] A. A. Aguilar-Arevalo *et al.* [MiniBooNE Collaboration], Phys. Rev. Lett. **102**, 101802 (2009) [arXiv:hep-ex/0812.2243].
 - [17] A. A. Aguilar-Arevalo *et al.* [MiniBooNE Collaboration], [arXiv:hep-ex/0904.1958].
 - [18] P. Adamson *et al.*, Phys. Rev. Lett. **102**, 211801 (2009) [arXiv:hep-ex/0809.2447].
 - [19] M. Maltoni, T. Schwetz, M. Tortola and J. W. F. Valle, New J. Phys. **6**, 122 (2004) [arXiv:hep-ph/0405172].
 - [20] A. A. Aguilar-Arevalo *et al.* [MiniBooNE Collaboration], Phys. Rev. D **79**, 072002 (2009) [arXiv:hep-ex/0806.1449].
 - [21] A. A. Aguilar-Arevalo *et al.* [MiniBooNE Collaboration], Nucl. Instrum. Meth. A **599**, 28 (2009) [arXiv:hep-ex/0806.4201].
 - [22] V. Barger, Y. B. Dai, K. Whisnant and B. L. Young, Phys. Rev. D **59**, 113010 (1999) [arXiv:hep-ph/9901388].
 - [23] B. Kayser, [arXiv:hep-ph/0211134].

- [24] P. Brâemaud, *Markov chains: Gibbs fields, Monte Carlo simulation, and queues*, Springer, New York, 1999.
- [25] M. Maltoni and T. Schwetz, Phys. Rev. D **68**, 033020 (2003) [arXiv:hep-ph/0304176].
- [26] A. A. Aguilar-Arevalo *et al.* [MiniBooNE Collaboration], arXiv:0903.2465 [hep-ex].
- [27] A. A. Aguilar-Arevalo *et al.* [SciBooNE Collaboration], arXiv:hep-ex/0601022.
- [28] K. B. M. Mahn, private communication.
- [29] I. Ambats *et al.* [MINOS Collaboration], FERMILAB-DESIGN-1998-02.
- [30] MINOS, J. Hartnell, (2009), FNAL Seminar, 15 May 2009.
URL:<http://theory.fnal.gov/jetp/talks/Hartnell.pdf>.
- [31] A. D. Sakharov, Pisma Zh. Eksp. Teor. Fiz. **5**, 32 (1967) [JETP Lett. **5**, 24 (1967 SOPUA,34,392-393.1991 UFNAA,161,61-64.1991)].
- [32] G. Barenboim and J. D. Lykken, Phys. Lett. B **554**, 73 (2003) [arXiv:hep-ph/0210411].
- [33] S. Hollenberg and H. Pas, arXiv:0904.2167 [hep-ph].
- [34] This constraint is imposed under the assumption that mixing with sterile neutrinos should be small.